This is a peer-reviewed, accepted author manuscript of the following research article: Alsalami, F. M., Benkhelifa, F., Ashour, D., Ghassemlooy, Z., Haas, O. C. L., Ahmad, Z., & Rajbhandari, S. (2023). Average channel capacity bounds of a dynamic vehicle-to-vehicle visible light communication system. IEEE Transactions on Vehicular Technology. https://doi.org/10.1109/TVT.2023.3320889

Average Channel Capacity Bounds of a Dynamic Vehicle-to-Vehicle Visible Light Communication System

Farah Mahdi Alsalami, Fatma Benkhelifa, *Member, IEEE*, Danah Ashour, Zabih Ghassemlooy, *Senior Member, IEEE*, Olivier C.L. Haas, Zahir Ahmad, and Sujan Rajbhandari, *Senior Member, IEEE*

***Abstract*—As vehicles trajectories are unpredictable and changing dynamically, vehicle-to-vehicle visible light communication (V2V-VLC) experiences a dynamic channel. In this work, we conduct measurements taking into account different realistic inter-vehicle distances and ambient noise levels at different times of the day in order to model and verify the dynamic V2V-VLC channel. We also derive the average channel capacity bounds by considering the impact of traffic at different times of the day, atmospheric turbulence and fog. Considering both peak and average optical power levels constraints, we derive the upper and lower bounds by using sphere packing and constraint relaxation methods, as well as truncated-exponential and truncated Gaussian distributions, respectively. The results show that the constraint relaxation method provides an improved estimation for the upper bound, whereas the truncated exponential distribution tightens the lower bound with a minimum gap of 0.4 bit/s/Hz during rush hour and in a clear weather condition. We also show that the average capacity bounds of V2V-VLC are less affected by atmospheric turbulence and fog, and that the capacity during rush hours is higher by 0.7 bit/s/Hz than during late hours.**

***Index Terms*—dynamic traffic conditions, dynamic vehicular traffic density, vehicular visible light communication (VVLC), channel model, vehicular communications, visible light communication (VLC).**

I. Introduction

Vehicle-to-vehicle (V2V) communication is part of traffic management technologies that aims to reduce congestion, CO_2 emission, and road accidents [1]. Several radio frequency (RF)-based technologies were proposed to connects vehicles, including dedicated short-range communications (DSRC), IEEE 802.11p, and LTE-V2V [2]. However, due to the high-demand on RF-based communication, these technologies are prone to interference and bandwidth limitation [3]–[5]. V2V visible light communication (V2V-VLC), is complementary to RF-based wireless schemes, which utilizes the front and taillights of vehicles to support ubiquitous V2V communications with reduced co-band interference [5]. Hence, it refocuses the use of RF spectrum to other applications.

V2V-VLC links are geometry-dependent due to the street layouts, vehicles types, and front and taillights configurations [5], [6]. This work investigates the use of headlights to enable V2V-VLC and to determine the channel capacity at different times of day. The irregular radiation patterns of headlights adds a random factor to geometric changes caused by vehicle movement. In addition, the channel experiences fluctuating gain and fading as a result of vehicles movement at different speeds as well as different weather conditions (i.e., turbulence), respectively.

Furthermore, when estimating the channel capacity (C_{cap}) of V2V-VLC both average and peak power constraints as well as the random channel gain due to mobility and turbulence needs considering.

The following section reviews the literature on V2V-VLC capacity considering mobility, atmospheric turbulence (AT), weather and transmitted optical peak and average power constraints.

A. Related Works

The impact of dynamic traffic, weather conditions including atmospheric turbulence (AT) on the V2V-VLC channel have been studied in the literature [7]–[11]. Due to the AT, the optical power fluctuates randomly as a result of signal fading [7], [11]–[13]. The performance of V2V-VLC with AT was modeled by a gamma-gamma distribution and using aperture averaging (AA) [11]. It was shown that AA stabilizes the system performance under AT conditions. Due to the relatively short inter-vehicular transmission range in V2V-VLC systems, in [7] a log-normal model was used to describe turbulence. The study also considered the impact of weather and shadowing. It was shown that receivers (Rxs) with hemispherical lens maximize the signal-to-noise ratio (SNR).

In [14]–[17], the average channel capacity (C_{avg}) of an optical wireless communication (OWC) link considering different AT models were investigated. A fixed point-to-point optical link was considered without accounting for peak and average optical power constraints.

The works in [18]–[25] focused on the tight upper and lower bounds for C_{cap} with Gaussian noise and under the

F. M. Alsalami, D. Ashour and Z. Ahmad are with the Faculty of Engineering, Environment and Computing, Coventry University, Coventry CV1 5FB, UK. (E-mail: ad9051@coventry.ac.uk, fatma.benkhelifa@kaust.edu.sa., ab7175@coventry.ac.uk)

F. Benkhelifa is with School of Electronic Engineering and Computer Science, Queen Mary University of London, London E1 4NS, UK, (e-mail: fatma.benkhelifa@kaust.edu.sa).

Z. Ghassemlooy is with the Optical Communications Research Group, Faculty of Engineering and Environment, Northumbria University, Newcastle upon Tyne, NE1 8ST, U.K. (e-mail: z.ghassemlooy@northumbria.ac.uk).

O.C.L. Haas is with the Centre for Future Transport and Cities (CFTC), Coventry University, Coventry CV1 5FB, UK. (E-mail: o.haas@coventry.ac.uk).

S. Rajbhandari is with the school of Computer Science and Electronic Engineering, Bangor University, Bangor, LL57 1UT, UK (E-mail: s.rajbhandari@bangor.ac.uk)

peak and average power constraints. Maximizing the mutual information between the channel input and output under positive and average optical intensity constraints over all possible input distributions was used to derive the lower bound of C_{cap}. The study in [19] used the continuous input with truncated-exponential distribution to determine the lower bound. In [24], a truncated-Gaussian distributed input was proposed to determine the lower bound. However, the study in [25] showed the capacity achieving probability measure is discrete for a conditionally Gaussian channel with bounded-input constraints.

Three methods are used to derive the capacity upper bounds, which are sphere packing; duality; and constraint relaxation. Sphere packing is a common method used to determine the communication channel capacity, which states that if a codeword is transmitted through a channel, then the received vector is contained in a sphere around the transmitted codeword [23], [24]. In [21], and [22], the sphere-packing upper bound argument method was used to show that there is a gap of at least 0.5 bit per transmission between lower- and upper-bounds on C_{cap}, which approaches zero at higher optical SNR. However, in [23], the gap between the upper- and lower-bounds derived in [21], and [22] was attributed to the mathematical approximation inaccuracies of the intrinsic volumes of the simplex. Therefore, in [23] alternative mathematical approximations of the intrinsic volumes of the simplex were proposed to derive a tight upper bound at higher SNR. In [26], the output entropy was considered to be larger than the input entropy for a point-to-point indoor signal-dependent Gaussian noise VLC channel. The channel capacity derivation solved the optimal input probability density function (PDF) optimization problem by using the variational method. In [19], the duality method was adopted to derive dual expressions for the upper bound for a free space optical link. Note, to derive the upper bound in [24], and [19]; the input constraints were relaxed to a variance constraint by finding the channel input distribution, which maximized the mutual entropy between the channel input and output.

In [27], the well-known water-filling principle, which relies on a Gaussian distribution of the signal at the channel input, was adopted to determine the theoretical C_{cap} upper bound for a perfectly linear optical transmission system. The study relied on the electro-optical nonlinearities compensation techniques to achieve linearity in VLC using commercial light emitting diodes. Similarly, the works in [15], [19], [28], and [29] considered the classical capacity $C = W \log_2(1 + \text{SNR})$, where W is the channel bandwidth and SNR is the received instantaneous electrical SNR, to provide an approximation of the maximum achievable data rate for a strictly linear system. In addition, channel model is band-limited with a defined bandwidth when the power dissipation by the DC component is excluded.

Most of the previous studies considered static VLC systems to derive closed-form expressions for C_{cap}. Limited works have investigated the impact of mobility on C_{cap} of outdoor VLC systems, particularly in V2V-VLC [30].

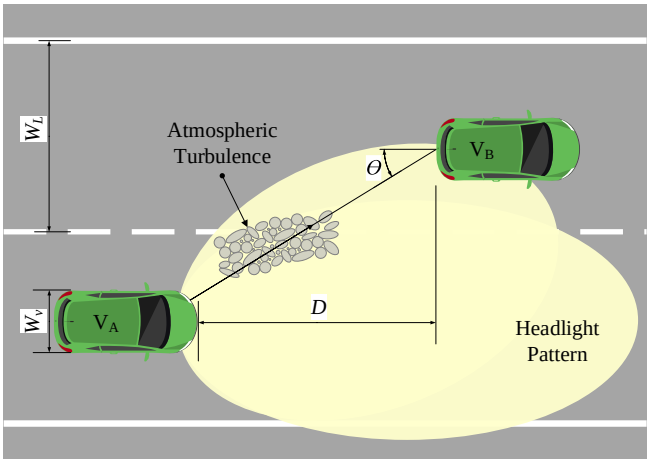

Fig. 1: A typical V2V-VLC link between a transmitting vehicle V_A using its headlight as Txs to send data to the vehicle in front V_B. The VLC link can experience atmospheric turbulence and fog.

B. Motivation and Original Contribution

The motivation of this study is to investigate the C_{cap} of a V2V-VLC link in a realistic outdoor environment by considering the dynamic traffic and atmospheric conditions (i.e., turbulence and fog). To the best of author's knowledge, no works have been reported on the link capacity considering the dynamic vehicle separations under different traffic conditions.

The novelty and original contributions of this study are as follows:

- Conduct experimental channel measurements to model the dynamic V2V channel. Measurements are conducted at different times of the day considering realistic inter-vehicle distances and ambient noise levels. Based on realistic traffic measurements from motorways (i.e., M6 and M42) in the UK, the inter-vehicle distance values are determined.
- Consider a non-negative real value of the optical signal and the average optical power constraints in VLC to derive the closed-form expression for the average lower- and upper-bound on V2V-VLC C_{cap}.
- Study the impact of vehicle mobility and dynamic traffic, headlight radiation patterns, and weather conditions (i.e., fog and turbulence) on the average bounds of C_{cap}.
- Compare sphere packing and constraint relaxation methods to derive the closed-form expression for the upper bound of C_{cap}.
- Compare truncated-exponential and truncated Gaussian distributions to derive the closed-form expression for the lower bound of C_{cap}.

The rest of the paper is organized as follows. The V2V-VLC channel model is presented in Section II. The V2V-VLC C_{cap} bounds are derived in Section III. Numerical results are discussed in Section IV. Finally, conclusions are drawn in Section VI.

II. V2V-VLC CHANNEL MODEL

A typical V2V-VLC link is shown in Fig. 1. It consists of a transmitting vehicle V_A using its headlight as Txs to send data to the vehicle in front V_B with a photo-detector (PD)-based Rx. Note, (i) the data signal can be information from the roadside infrastructure or the vehicles behind V_A; (ii) vehicle headlights have asymmetrical radiation patterns, which cannot be described by the traditional Lambertian model; and (iii) vehicles are driving in a realistic outdoor environment with dynamic traffic, atmospheric turbulence and weather conditions.

The transmitted intensity modulated optical signal composed of m independent symbols $\mathbf{X}$=(X_1,X_2,..., X_m) propagates through a free-space channel with a variable gain of h_t. The received signal is expressed as [31]:

$$\mathbf{Y} = h_t\mathbf{X} + \mathbf{n}; \tag{1}$$

where $\mathbf{n}$ represents the additive white Gaussian noise (AWGN) vector with zero mean and standard deviation σ_n, which represent all noise sources. The channel gain is given as in [14], [17], [32]:

$$h_t = h_g h_a h_w; \tag{2}$$

where h_g represents geometrical changes as a result of vehicles' speed and headlight radiation patterns, h_a and h_w represent atmospheric turbulence and fog, respectively. Note the channel gain is subject to random fluctuations, but its coherence time τ_c is normally in the range of milliseconds [33], [34], which is considerably shorter than the data symbol duration (typically in the range of micro-to-nanoseconds), e.g., considering sampling rate values of 200 kHz and 200 MHz, respectively in [33], [34]. Hence, the V2V-VLC channel can be considered as a block slow-fading channel, and therefore h_t is considered to be flat [14], [32].

The work in [30] developed a V2V-VLC path loss model, which is equivalent to h_g, and considered the impact of both vehicles' mobility and the headlight designs. The study used (i) realistic traffic measurements to describe the mobility and inter-vehicular distance during the late (0:00-3:00) and rush (12:00-15:00) hours; and (ii) the empirical radiation pattern of Toyota Altis headlight provided in [35], [36]. For the V2V-VLC channel, the resulting path loss (in dB) is given as [30]:

$$P_L(x;\mu_c,\sigma_c) = \frac{173}{(2\pi)^{(3/2)}\theta_o\sigma_c} \int_{\alpha_{\text{cmin}}}^{\alpha_{\text{cmax}}} \frac{\exp\left(-\frac{(x-y-\mu_c)^2}{\sigma_c^2}\right)}{\sqrt{3985.4-y^2}}\, dy \tag{3}$$

where the incident angle $\theta \sim U(0,\theta_o)$ varies between 0 and the maximum incident angle of θ_o. The integral boundaries are given as $\alpha_{\text{cmin}} = 63.13\cos(2\pi(\theta_o)/173)$ and $\alpha_{\text{cmax}} = 63.13\cos(2\pi(\theta_o+90)/173)$, $\sigma_c = 49.49\sigma_d/\log(10)$ and $\mu_c = 695.3 - 49.49\mu_d/\log(10)$, where σ_d and μ_d are the parameters of the distribution related to the inter-vehicular distance. The results in [30] also showed that the path loss in V2V-VLC can be closely approximated by a normal distribution. Hence, h_g is defined by a logarithmic transformation

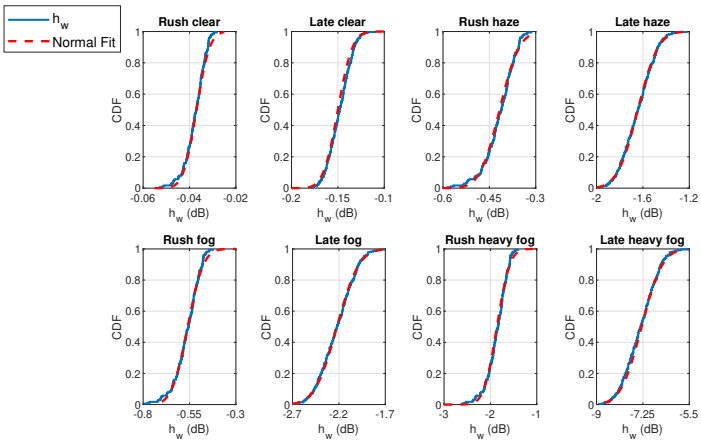

Fig. 2: The CDF of h_w for propagation distance varies according to the inter-vehicular distance values on M6 and M42 motorways at the rush and late hours from (12:00-15:00) and (0:00-03:00), respectively.

of the path loss, which is given by a log-normal distribution with parameters μ_g and σ_g:

$$P_{h_g}(g) = \frac{1}{\sigma_g\sqrt{2\pi}}\frac{1}{g}\exp\Big(-\frac{(\log(g)-\mu_g)^2}{2\sigma_g^2}\Big). \tag{4}$$

In most V2V systems with a short transmission range the weak turbulence regime is considered, and h_a is modeled by a log-normal distribution [7], with parameters μ_a and σ_a:

$$P_{h_a}(h_a) = \frac{1}{\sigma_a\sqrt{2\pi}}\frac{1}{h_a}\exp\Big(-\frac{(\log(h_a)-\mu_a)^2}{2\sigma_a^2}\Big). \tag{5}$$

The impact of h_w on static OWC was studied in [37]. The works in [14], and [17] considered weather impact to determine the average C_{cap}. The atmospheric losses due to weather conditions are modelled by Beer-Lambert law for a fixed transmission range, where h_w depends on the visibility range [37] as given by:

$$h_w = e^{-LA_{dw}(\lambda)} \tag{6}$$

where L is the propagation distance and $A_{dw}(\lambda)$ is the attenuation coefficient due to different weather conditions. The coefficient $A_{dw}(\lambda)$ (in dB/km) is given as [38], [39]:

$$A_{dw}(\lambda) = \frac{17.35}{l}\Big(\frac{\lambda}{550}\Big)^{-\eta} \qquad (dB/km) \tag{7}$$

where l is the visibility range and η is a visibility range-dependent parameter for different weather conditions [39]. The V2V-VLC channels are dynamic and subject to varying transmission ranges. The mean transmission range (i.e., the inter-vehicular distance) values during rush and late hours are 12.37 m and 48.72 m, respectively [30]. As can be seen from Table I, the impact of different weather conditions becomes more significant for longer distances (in Km). Fig. 2 shows the cumulative distribution functions (CDF) of h_w (dB) in (6) as a function of varying inter-vehicular distances during the rush and late hours of (12:00-15:00) and (0:00-03:00), respectively. The figure illustrates that h_w (dB) fits the normal distribution (i.e., h_w has a log-normal distribution in

TABLE I: Attenuation values under different weather conditions [39] and parameters of h_w distribution.

Weather Condition	Visibility range (km)	A_{dw} (dB/km)	(μ_w, σ_w) Late	(μ_w, σ_w) Rush
Clear	20	0.7	-0.037, 0.005	-0.15, 0.012
Haze	2	7.77	-0.417, 0.050	-1.64, 0.138
Thin fog	1.5	10.5	-0.560, 0.067	-2.22, 0.187
Heavy fog	0.5	34.69	-1.863, 0.223	-7.33, 0.616

the normal scale) with the parameters given in Table I, which shows that the standard deviation value σ_w under different weather and traffic conditions are low, i.e., h_w values are clustered around the mean value. Note the short transmission distance in V2V (i.e., tens of meters) means that the variation in received power (i.e., standard deviation in Table I) caused by atmospheric conditions is relatively small compared to the power variation due to geometrical losses and turbulence. Therefore , we assume that, except for the additional attenuation parameter μ_w, i.e., $\mu_{h_t} = \mu_a\mu_g + \mu_w$ weather conditions do not affect channel gain distribution [8].

Considering that the random variation of the gain due to h_g is independent of h_a, the channel gain in (2) can be described by a log-normal distribution with parameters $\mu_{h_t} = \mu_a\mu_g+\mu_w$ and $\sigma_{h_t} = (\sigma^2_{h_g}\sigma^2_{h_a} + \mu^2_{h_g}\mu^2_{h_a}) - \mu^2_{h_g}\mu^2_{h_a}$ [40]:

$$P_{h_t}(h_t) = \frac{1}{\sigma_{h_t}\sqrt{2\pi}}\frac{1}{h_t}\exp\Big(-\frac{(\log(h_t)-\mu_{h_t})^2}{2\sigma^2_{h_t}}\Big). \quad (8)$$

Because the channel is randomly varying, C_{cap} must be considered as a random variable. Thus, the average capacity value is calculated to indicate the average best rate for error-free transmission [15], [41].

III. V2V-VLC CHANNEL CAPACITY

The optical average and peak power of the transmitted signal X (which is the channel input) are constrained due to the eye safety and other practical considerations. The optical peak power A and the average optical power must meet the following constraint [19], [32]:

$$P_r[X > A] = 0, \quad (9)$$

$$E[X] \leq \varepsilon; \quad (10)$$

where ε is a constant.

In addition, the ratio between ε and A is defined as:

$$\alpha \triangleq \frac{\varepsilon}{A}. \quad (11)$$

where $\alpha \in$[0,1].

Considering a memoryless V2V-VLC channel, C_{cap} $C(A,\varepsilon)$ is given by the supremum of the mutual information between the channel input X and output Y over all laws as:

$$C(A,\varepsilon) = \sup_{\mathbb{P}_X} I(X,Y) = \sup_{\mathbb{P}_X} I(X, h_t\mathbf{X}+\mathbf{n}). \quad (12)$$

where $\mathbb{P}_X$ is the distribution of X.

Note that, (12) shows that the mutual information between X and Y is affected by h_t. Since the V2V-VLC channel is a random time-varying channel, we must consider the random variation of the channel to find the average achievable rate with the arbitrarily small probability of error [15], [17]. Hence, C_{avg} (also known as ergodic capacity) is given by [17]:

$$C_{\text{avg}} = \langle C(A,\varepsilon)\rangle = \int_0^\infty C(A,\varepsilon)P_{h_t}(h_t)dh_t. \quad (13)$$

In the following sections, we present upper and lower bounds on C_{avg} $\langle C(A,\varepsilon)\rangle$ using different methods and considering A and ε constraints.

A. The average capacity lower bound

The entropy-power inequality (EPI) is used to determine the lower bound on C_{cap} [19], [32], [42], which is given by:

$$\begin{aligned} C(A,\varepsilon) &\geq I(X,Y) \\ &= h(Y) - h(Y|X) \\ &= h(h_t\mathbf{X}+\mathbf{n}) - h(\mathbf{n}) \\ &= \frac{1}{2}\log\Big(e^{2h(h_t\mathbf{X})} + e^{2h(\mathbf{n})}\Big) - h(\mathbf{n}) \\ &= \frac{1}{2}\log\Big(\frac{h_t^2 e^{2h(\mathbf{X})}}{2\pi\sigma_n^2 e} + 1\Big). \end{aligned} \quad (14)$$

Note that from (14), the lower bounds can be found by choosing an input distribution $\mathbb{P}_X$ that maximizes the entropy $h(X)$. To determine the tight bounds both continuous and discrete input distributions are proposed. In this work, we focus only on continuous input distributions as outlined below.

1) Truncated-Exponential and Uniform Input Distributions: The work in [19] proposed using truncated-exponential and uniform input distributions $\mathbb{P}_X$ to maximize the entropy $h(X)$ under the peak and average constraints. As a result, the lower bound on the C_{cap} is given as [19], [32]:

$$C(A,\varepsilon) \geq \begin{cases} \frac{1}{2}\log\left(1 + \frac{h_t^2A^2e^{2\mu^*}}{2\pi e\sigma_n^2}\left(\frac{1-e^{-\mu^*}}{\mu^*}\right)^2\right), for \quad \alpha < \frac{1}{2} \\ \log\left(1+\frac{h_t^2A^2}{2\pi e\sigma_n^2}\right), \qquad\qquad for \quad \alpha = \frac{1}{2} \end{cases} \quad (15)$$

where $\mu^* > 0$ is a unique solution of $\frac{1}{\mu^*} - \frac{e^{-\mu^*}}{1-e^{-\mu^*}} = \frac{\varepsilon}{A}$.

Using (8), (13) and (15), the average capacity is calculated by solving (16) (given at the bottom of the next page).

Using $z = \log(h_t)$, $\omega_e = \frac{A^2}{2\pi e\sigma_n^2}e^{2\mu^*}$, $\omega_d = \frac{A^2}{2\pi e\sigma_n^2}$, $\mu_e = \mu_{h_t} + 0.5\log(\omega_e)$ and $\mu_d = \mu_{h_t} + 0.5\log(\omega_d)$, (16), is re-written as:

$$\langle C(A,\varepsilon)\rangle \geq \frac{1}{2\sigma_{h_t}\sqrt{2\pi}} \begin{cases} \int_0^\infty \log(1+e^{2z}) \\ \exp\Big(-\frac{(z-\mu_e)^2}{2\sigma^2_{h_t}}\Big)dz, for \quad \alpha < \frac{1}{2} \\ \\ \int_0^\infty \log(1+e^{2z}) \\ \exp\Big(-\frac{(z-\mu_d)^2}{2\sigma^2_{h_t}}\Big)dz, for \quad \alpha = \frac{1}{2} \end{cases} \quad (17)$$

Using the equality $\log(1+e^{2y}) = \sum_{k=1}^{+\infty}(-1)^{k+1}y^{2k}/k$ and the definition of the scaled complementary error function

$\mathrm{erfcx}(y) = \exp(y^2)\mathrm{erfc}(y)$ [15], [43], the integral in (17) is solved as:

$$\langle C(A,\varepsilon)\rangle \geq 0.5\exp\left(\frac{\mu_e}{2\sigma_{h_t}^2}\right)\sum_{k=1}^{+\infty}\frac{(-1)^{k+1}}{k}\left[\mathrm{erfcx}\left(\frac{\sigma k}{\sqrt{2}}+\frac{\mu_e}{\sqrt{2}\sigma_{h_t}}\right)+\mathrm{erfcx}\left(\frac{\sigma k}{\sqrt{2}}-\frac{\mu_e}{\sqrt{2}\sigma_{h_t}}\right)\right]+\frac{2\sigma}{\sqrt{2\pi}}\exp\left(\frac{\mu_e}{2\sigma_{h_t}^2}\right)+(\mu_e)\mathrm{erfc}\left(\frac{\mu_e}{\sqrt{2}\sigma_{h_t}}\right), \quad (18)$$

for $\alpha < \frac{1}{2}$, and

$$\langle C(A,\varepsilon)\rangle \geq 0.5\exp\left(\frac{\mu_d}{2\sigma_{h_t}^2}\right)\sum_{k=1}^{+\infty}\frac{(-1)^{k+1}}{k}\left[\mathrm{erfcx}\left(\frac{\sigma k}{\sqrt{2}}+\frac{\mu_d}{\sqrt{2}\sigma_{h_t}}\right)+\mathrm{erfcx}\left(\frac{\sigma k}{\sqrt{2}}-\frac{\mu_d}{\sqrt{2}\sigma_{h_t}}\right)\right]+\frac{2\sigma}{\sqrt{2\pi}}\exp\left(\frac{\mu_d}{2\sigma_{h_t}^2}\right)+(\mu_d)\mathrm{erfc}\left(\frac{\mu_d}{\sqrt{2}\sigma_{h_t}}\right), \quad (19)$$

for $\alpha = \frac{1}{2}$.

2) Truncated-Gaussian Distribution: The work in [24] used truncated-Gaussian distribution to calculate the lower bound on C_{cap} because Gaussian distribution achieves the capacity of the AWGN channel. The resulting lower bound on the C_{cap} is given by (20) at the bottom of the next page (where, $\mathbb{P}^G_{\tilde{\mu},\tilde{\nu}}(x)$ and $\mathbb{F}^G_{\tilde{\mu},\tilde{\nu}}(x)$ are the PDF and CDF of the input Gaussian distribution with a mean and standard deviation of $(\tilde{\mu},\tilde{\nu})$).

for $\tilde{\nu} = \frac{\tilde{\mu}}{3}$ and $\tilde{\mu} < \varepsilon$, the suboptimal lower bound [32] and its average capacity are given respectively as:

$$C(A,\varepsilon) \geq \frac{1}{2}\log\left(1+\frac{h_t^2\varepsilon^2}{2\pi e\sigma_n^2}\right); \quad (21)$$

and

$$\langle C(A,\varepsilon)\rangle = \frac{1}{2\sigma_{h_t}\sqrt{2\pi}\log(2)}\int_0^{\infty}\frac{1}{h_t}\log\left(1+\frac{h_t^2\varepsilon^2}{\sigma_n^2}\right)\exp\left(-\frac{(\log(h_t)-\mu_h)^2}{2\sigma_{h_t}^2}\right)dh_t. \quad (22)$$

Following the same derivation steps in (18), the average lower bound can be written as:

$$\langle C(A,\varepsilon)\rangle \geq 0.5\exp\left(\frac{\mu_j}{2\sigma_{h_t}^2}\right)\sum_{k=1}^{+\infty}\frac{(-1)^{k+1}}{k}\left[\mathrm{erfcx}\left(\frac{\sigma k}{\sqrt{2}}+\frac{\mu_j}{\sqrt{2}\sigma_{h_t}}\right)+\mathrm{erfcx}\left(\frac{\sigma k}{\sqrt{2}}-\frac{\mu_j}{\sqrt{2}\sigma_{h_t}}\right)\right]+\frac{2\sigma}{\sqrt{2\pi}}\exp\left(\frac{\mu_j}{2\sigma_{h_t}^2}\right)+(\mu_j)\mathrm{erfc}\left(\frac{\mu_j}{\sqrt{2}\sigma_{h_t}}\right), \quad (23)$$

where $\mu_j = \mu_{h_t} + \log\left(\frac{\varepsilon}{\sqrt{(2\pi e)}\sigma_n}\right)$.

Having calculated the average capacity lower bound, the average capacity upper bound is derived in the following section.

B. Average capacity upper bound

In this study, we consider two methods to calculate the average capacity upper bound on the V2V-VLC channel: sphere packing and constraint relaxation.

1) Sphere Packing Average Capacity Upper Bound: The upper bound on C_{cap} of VLC is given by [44]:

$$C(A,\varepsilon) \leq \log_2\left(\frac{\left(\frac{e}{2\pi}\right)^{\frac{c^*}{2}}\gamma^{\frac{-c^*}{\beta}}}{(c^*)^{2c^*}(1-c^*)^{\frac{3}{2}(1-c^*)}}\left(\frac{h_t\varepsilon}{\sigma_n}\right)^{c^*}\right), \quad (24)$$

where the numerical coefficients γ=0.74 and β=1.75 were determined to tighten the lower bound on the complementary error function and the optimized parameter $c^* \in [0,1]$ satisfies:

$$2\log_2(c^*) - \frac{3}{2}\log_2(1-c^*) = -\frac{1}{\log 4}+\frac{1}{2}\log_2\left(\frac{e}{2\pi}\right)-\frac{1}{\beta}\log_2(\gamma)+\log_2\left(\frac{h_t\varepsilon}{\sigma_n}\right). \quad (25)$$

Using (8), (13) and (24), the average capacity upper bound can be calculated as:

$$\langle C(A,\varepsilon)\rangle = \frac{1}{\sigma_{h_t}\sqrt{2\pi}\log(2)}\int_0^{\infty}\log\left(\frac{\left(\frac{e}{2\pi}\right)^{\frac{c^*}{2}}\alpha^{\frac{-c^*}{\beta}}}{(c^*)^{2c^*}(1-c^*)^{\frac{3}{2}(1-c^*)}}\left(\frac{h_t\varepsilon}{\sigma_n}\right)^{c^*}\right)\frac{1}{h_t}\exp\left(-\frac{(\log(h_t)-\mu_h)^2}{2\sigma_{h_t}^2}\right)dh_t. \quad (26)$$

The solution of (26) is given as:

$$\langle C(A,\varepsilon)\rangle \leq \frac{\bar{c}^*\mu_m}{\log(2)}+\frac{\bar{c}^*}{\log(2)}\log\left(\frac{\left(\frac{e}{2\pi}\right)^2\alpha^{-1/\beta}}{(\bar{c}^*)^2(1-\bar{c}^*)^{3(1-\bar{c}^*)/2\bar{c}^*}}\left(\frac{\varepsilon}{\sigma_n}\right)\right), \quad (27)$$

$$\langle C(A,\varepsilon)\rangle \geq \frac{1}{2\sigma_{h_t}\sqrt{2\pi}}\begin{cases}\int_0^{\infty}\frac{1}{h_t}\log\left(1+\frac{h_t^2A^2}{2\pi e\sigma_n^2}e^{2\mu^*}\left(\frac{1-e^{-\mu^*}}{\mu^*}\right)^2\right)\exp\left(-\frac{(\log(h_t)-\mu_{h_t})^2}{2\sigma_{h_t}^2}\right)dh_t, & for \quad \alpha<\frac{1}{2}\\ \int_0^{\infty}\frac{1}{h_t}\log\left(1+\frac{h_t^2A^2}{2\pi e\sigma_n^2}\right)\exp\left(-\frac{(\log(h_t)-\mu_{h_t})^2}{2\sigma_{h_t}^2}\right)dh_t, & for \quad \alpha=\frac{1}{2}\end{cases} \quad (16)$$

where the optimized parameter $\bar{c}^*$ is given by:

$$2\log_2(\bar{c}^*) - \frac{3}{2}\log_2(1-\bar{c}^*) = \mu_m - \frac{1}{\log 4} + \frac{1}{2}\log_2\left(\frac{e}{2\pi}\right) - \frac{1}{\beta}\log_2(\alpha) + \log_2\left(\frac{\varepsilon}{\sigma_n}\right). \quad (28)$$

Note that only the average power constraint is considered using sphere packing to derive the upper bound on C_{cap} [44], and [32].

2) Constraint relaxation: Considering that $\mathbf{X}$ is a random variable which meets the peak and average constraints in (9) and (10), the maximum variance of the input $E[(X_i - E[X_i])^2] = \varepsilon(A-\varepsilon)$ is achieved by a binary distribution $\mathbb{P}_X = (1-\frac{\varepsilon}{A})\delta(X) + \frac{\varepsilon}{A}\delta(X-A)$ [24], [32]. Hence, the upper bound on C_{cap} is given by [19], [32]:

$$C(A,\varepsilon) \leq \log\left(1 + \varepsilon(A-\varepsilon)\frac{h_t^2}{\sigma_n^2}\right). \quad (29)$$

From (8), (13), and (29), the average capacity upper bound is given by the solution of the integration:

$$\langle C(A,\varepsilon)\rangle \leq \frac{1}{\sigma_{h_t}\sqrt{2\pi}}\int_0^\infty \frac{1}{h_t}\log\left(1+\alpha(1-\alpha)\frac{h_t^2A^2}{\sigma_n^2}\right) \exp\Big(-\frac{(\log(h_t)-\mu_h)^2}{2\sigma_{h_t}^2}\Big)dh_t. \quad (30)$$

Similar to (17), by changing the variables $y = \log(h_t)$ and $\omega_u = \alpha(1-\alpha)\frac{A^2}{\sigma_n^2}$ and following some manipulation, (30) is re-written as:

$$\langle C(A,\varepsilon)\rangle \leq \frac{1}{\sigma_{h_t}\sqrt{2\pi}}\int_0^\infty \log\left(1+e^{2y}\right) \exp\Big(-\frac{(y-\mu_u)^2}{2\sigma_{h_t}^2}\Big)dy. \quad (31)$$

where $\mu_u = \mu_{h_t} + 0.5\log(\omega_u)$.

Similarly, using the equality $\log(1+e^{2y}) = \sum_{k=1}^{+\infty}(-1)^{k+1}y^{2k}/k$ and $\text{erfcx}(y) = \exp(y^2)\text{erfc}(y)$ [15], [43], the integral in (31) is solved as:

$$\langle C(A,\varepsilon)\rangle \leq 0.5\exp\left(\frac{\mu_u}{2\sigma_{h_t}^2}\right)\sum_{k=1}^{+\infty}\frac{(-1)^{k+1}}{k} \left[\text{erfcx}\left(\frac{\sigma k}{\sqrt{2}} + \frac{\mu_u}{\sqrt{2}\sigma_{h_t}}\right) + \text{erfcx}\left(\frac{\sigma k}{\sqrt{2}} - \frac{\mu_u}{\sqrt{2}\sigma_{h_t}}\right)\right] + \frac{2\sigma}{\sqrt{2\pi}}\exp\left(\frac{\mu_u}{2\sigma_{h_t}^2}\right) + (\mu_u)\text{erfc}\left(\frac{\mu_u}{\sqrt{2}\sigma_{h_t}}\right) \quad (32)$$

The convergence analysis of (18), (19), (23), and (32) is provided in Appendix A.

The following section presents simulation results and discussions to examine the validity of the derivation and the obtained average capacity bounds.

IV. Results and discussion

As part of the modelling of the dynamic V2V system, we have measured the channel gain considering the realistic inter-vehicle distances and the ambient noise levels at different times of the day using the experimental setup depicted in Fig. 3. We have used headlights of Ford Fiesta 2002, where the original bulb is replaced with commercial LED lamps. Prior to the measurement, the headlights were adjusted in accordance with ECE R112 regulation. All key dimensions are shown in Fig. 3. An analog power meter console with a standard photodiode sensor (Thorlabs 100A and S120C) was mounted at a height of 640 mm above the ground facing headlights. Measurements were conducted on 8, 9, and 21 February 2023 from 12:00-2:00 and 17:30-19:30, which correspond to the rush and late hours, respectively, of the day. According to traffic data collected from the multiple-loop sensors on M42 and M6 on 21, 24, and 28 November and 6, 7, and 8 December 2017, respectively, the distances were measured. With a lane width of 3.65 m, the mean values of the distance for the rush (12.00-15.00) and late hours (00.00-03.00) of the day are D_{rush} = 12.37 m and D_{late} = 48.72 m, respectively. In order to estimate the distribution that best describes the received power, we applied a curve-fitting method based on Normal, log-normal, Gamma, and Nakagami distributions. The standard error values of the parameters of the distribution are used to evaluate the distribution fitting. In Table II, we provide the parameters for the Normal, log-normal, Nakagami, and Gamma distributions as well as their standard error values during rush and late hours. Among all distributions, the log-normal distribution provides the best fit with the least standard error, which matches well with the analytical expectation for the log-normal distribution for the channel gain in (8). Fig. 4 (a) shows the CDFs of the measured received power values along with the Normal, log-normal, Nakagami, and Gamma distributions during the rush and late hours. Note that Fig. 4 (b) confirms this result by showing the CDFs of the path loss (in dB), which fits a normal distribution given in [30] during the rush and late hours.

To validate the mathematical analysis in section III, we carry out a simulation-based study with parameter values shown in Table III. According to [32], it is sufficient to study the channel capacity for $\alpha < 0.5$, since a channel capacity with a peak constraint has similar properties to a channel with an average and peak constraints with $\alpha < 0.5$. Hence, we only considered the case for α <0.5 to investigate C_{avg}.

Fig. 5 illustrates the numerical average capacity using (16), (22), (26), and (31) as a function of the average optical SNR ε/σ_n for sphere packing and constraint upper bounds,

$$C(A,\varepsilon) = \max_{\tilde{\mu},\tilde{\nu}}\frac{1}{2}\log\Big(1+\frac{h_t^2\tilde{\nu}^2}{\sigma_n^2}\Big) + \log\left(\mathbb{F}^G_{\tilde{\mu},\tilde{\nu}}(A) - \mathbb{F}^G_{\tilde{\mu},\tilde{\nu}}(0)\right) - \frac{h_t^2\tilde{\nu}^2}{2(\mathbb{F}^G_{\tilde{\mu},\tilde{\nu}}(A) - \mathbb{F}^G_{\tilde{\mu},\tilde{\nu}}(0))(1+\frac{h_t^2\tilde{\nu}^2}{\sigma_n^2})}\Big((A-\tilde{\mu})\mathbb{P}^G_{\tilde{\mu},\tilde{\nu}}(A) - \tilde{\mu}\mathbb{P}^G_{\tilde{\mu},\tilde{\nu}}(0)\Big). \quad (20)$$

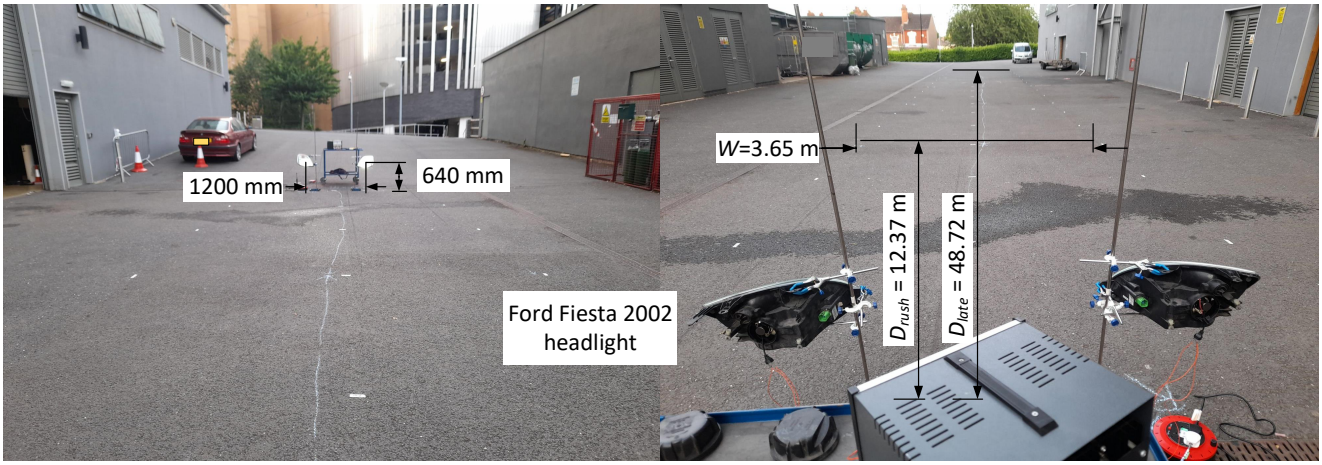

Fig. 3: The measurement setup.

TABLE II: Parameters for different distributions that are expected to describe the received power.

Time	Distribution	Mean value (W)	μ_d	Estimation error μ_d (%)	σ_d	Estimation error σ_d (%)
12:00-14:00 (rush hours)	log-normal	40.56 n	3.79	0.74	0.09	0.52
	Nakagami	40.56 n	28.85	274.00	1661.72	2470.27
	Normal	40.56 n	40.56	30.5	4.04	21.6
	Gamma	40.56 n	103.69	1106.67	0.39.13	4.19
17:30-19:30 (late hours)	log-normal	14.13 μ	0.2.52	2.91	0.50	2.07
	Nakagami	14.42 μ	1.12	8.23	258.29	1421.61
	Normal	14.16 μ	14.167	44.33	7.60	31.42
	Gamma	14.16 μ	4.08	32.366	3.47	29.32

TABLE III: Simulation parameters.

Symbol	Parameter	Values
σ_n^2	AWGN variance	10^{-14} [41]
μ_a	AT log-normal distribution parameter	0.4 [7]
σ_a^2	AT log-normal distribution parameter	0.8 [7]
μ_g	geometrical log-normal distribution parameter-Rush	-74.7 dB [30]
σ_g^2	geometrical log-normal distribution parameter-Rush	5.4 [30]
μ_g	geometrical log-normal distribution parameter-Late	-102.8 dB [30]
σ_g^2	geometrical log-normal distribution parameter-Late	3.2 [30]

as well as truncated-exponential and truncated-Gaussian lower bounds compared to plots obtained using (18), (23), (27), and (32) for $\varepsilon = A/4$ at rush hours during (12:00-15:00) and under a clear weather condition. As expected, the figure shows the adequacy between the results obtained by the analytical and numerical expressions. The figure also demonstrates (i) the truncated-Gaussian exhibits a tighter lower bound than others for all values of SNR, which is highly desirable in vehicular communications with different illumination levels; (ii) at the SNR $>$ 10 dB, sphere packing, which considers the average power constraint only, is characterized by a looser upper bound compared to other; and (iii) at SNR $<$ 4, dB sphere packing is tighter to the truncated-Gaussian lower bound. The constraint relaxation upper bound provides much improved realization of the upper bound on C_{cap}. However, the gap between the average upper bound obtained using constraint relaxation method and the average lower bound obtained using the truncated-exponential is $<$ 0.5 bit/s/Hz at low SNR values. The gap increases by up to 1 bit/s/Hz at high SNR values (i.e., $>$ 10 dB).

The impact of dynamic traffic on the VVLC average C_{cap} as a function of the average optical SNR ε/σ_n for the four bounds during the rush and late hours, under a clear weather condition, and for $\varepsilon = A/4$ bounds is depicted in Fig. 6. Note that, (i) all plots show lower values of 0.7 bit/s/Hz for the C_{avg} for late hours compared with rush hours. This is expected because the inter-vehicular distance is relatively longer at late night hours, and hence, the path loss values are larger [30]; (ii) the truncated-exponential lower bound show the tighter bound for both case; (iii) at lower optical SNR of $<$ 0 dB, sphere packing upper bond is closer to truncated-Gaussian and beyond the SNR of 2.5 dB it is much lighter bound compared with others, see Fig. 6(a); and (iv) during the late hours, sphere packing display the lighter bound for all values of optical SNR compared with the others. The figure shows that the constraint relaxation upper bound, truncated-Gaussian lower bound, and truncated-exponential lower bound have lower values of C_{avg} at late hours than rush hours, with the latter displaying the tighter bound in both figures. Due to the dynamic traffic environment, the sphere packing upper bound is less dependent on the channel variation. The reason for this is that the channel variation results in variation in peak power, which is not considered in the sphere packing method.

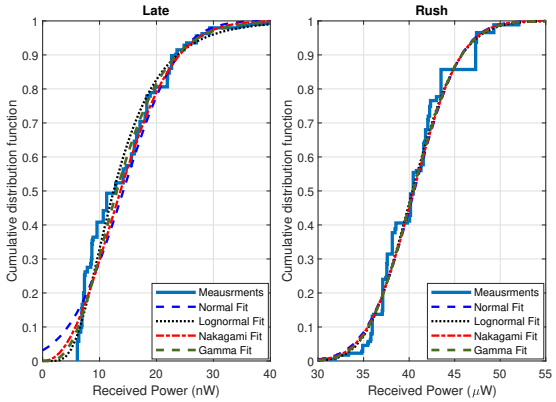

(a)

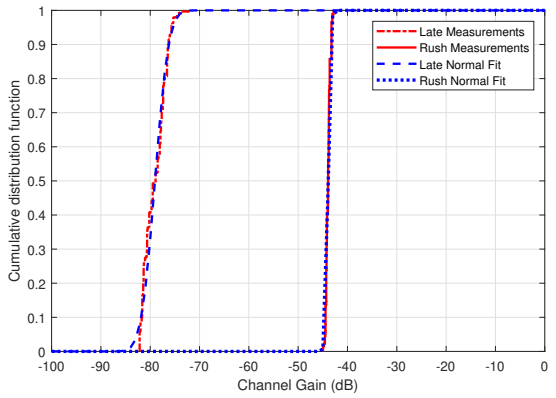

(b)

Fig. 4: The measured CDFs as a function of a channel gain for: (a) received power, and (b) channel gain during the rush and late hours.

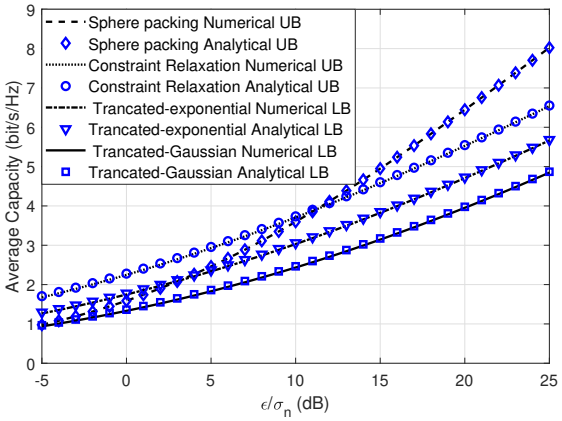

Fig. 5: C_{avg} vs. average SNR ε/σ_n for $\varepsilon = A/4$ at rush hours between 12:00-15:00 and under a clear weather condition.

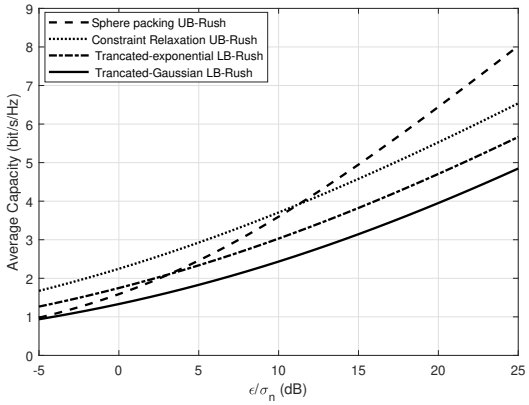

(a)

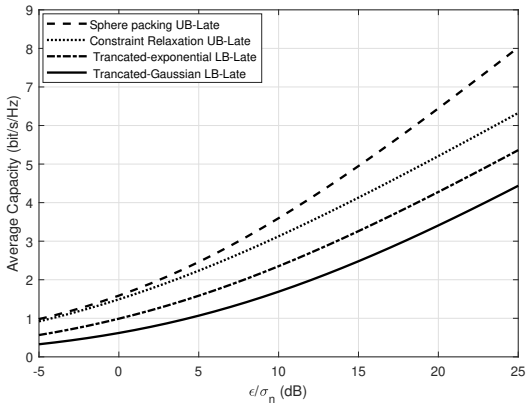

(b)

Fig. 6: The impact of dynamic traffic on VVLC average sphere packing upper bound, constraint relaxation upper bound, truncated-exponential lower bound and truncated-Gaussian lower bound at (a) rush hours (12:00-15:00) and (b) late hours (00:00-03:00) for $\varepsilon = A/4$ and clear weather.

Fig. 7 shows C_{avg} bounds given in (27), (32), (18), and (23) as a function of the peak optical SNR A/σ_n for a range of ε of $A/10$, $A/4$, and $A/2$ at rush hours and clear weather. The plots show the same patterns as in Figs. 5 and 6, with the average constraint relaxation upper bound and uniform distribution lower bound being tighter for $\varepsilon = A/2$, see Fig. 7(c).

The impact of AT on C_{avg} bounds against the average optical SNR ε/σ_n for all cases at rush hours, clear weather, and for $\varepsilon = A/4$ is illustrated in Fig. 8. The figure shows that the average sphere packing upper bound is not affected by the AT. However, the average constraint relaxation upper bound, truncated-exponential lower bound and the truncated-Gaussian lower bound display a drop in C_{avg} by 0.2 bit/s/Hz at low values between -5 dB and 5 dB under the AT regime. The difference decreases to 0.1 bit/s/Hz at high SNR values, i.e., the impact of AT can be reduced by increasing the SNR values. In general, the observed change in C_{avg} is insignificant for all SNR values and therefore, AT impact can be negligible.

Finally, Fig. 9 depicts the impact of weather on C_{avg} bound as a function of the average optical SNR ε/σ_n for all cases and for clear, haze, and heavy fog conditions during the rush

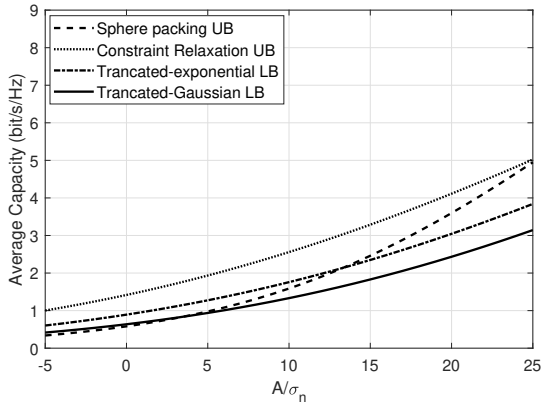

(a)

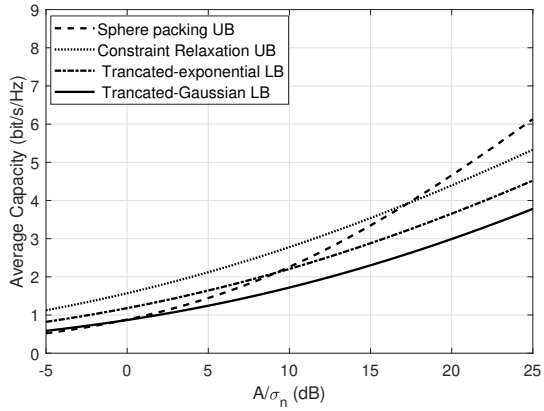

(b)

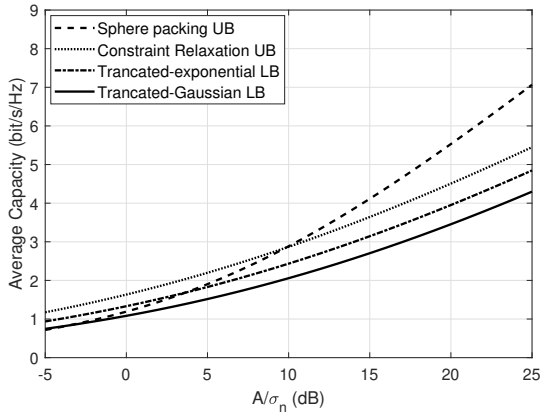

(c)

Fig. 7: C_{avg} vs. the peak optical SNR A/σ_n sphere packing upper bound, constraint relaxation upper bound, truncated-exponential lower bound and truncated-Gaussian lower bound for ε of (a) $A/10$, (b) $A/4$ and (c) $A/2$ at rush hours (12:00-15:00) and a clear weather condition.

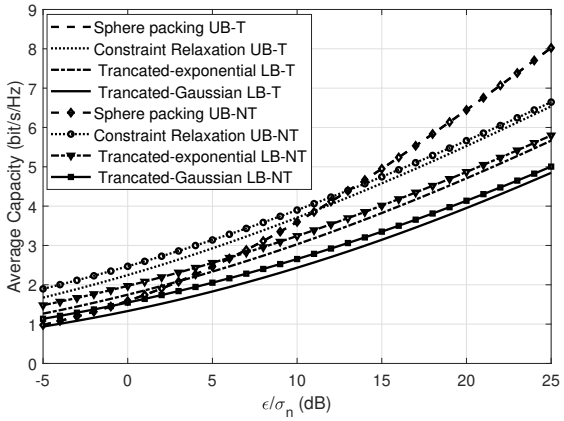

Fig. 8: Impact of AT on C_{avg} bounds with (T) and without (NT) turbulence conditions at rush hours, clear weather and when $\varepsilon = A/4$

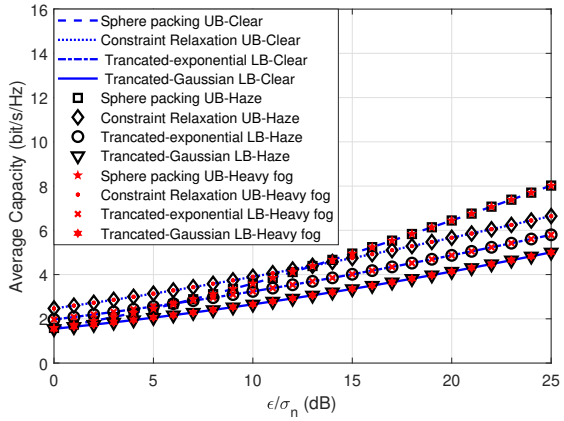

Fig. 9: C_{avg} bounds under selected weather conditions: clear, haze, and heavy fog at rush hours and for $\varepsilon = A/4$.

hours and for $\varepsilon = A/4$. The results show that different weather conditions do not have a noticeable impact on the achievable C_{avg}. This is because the mean value of the channel gain μ_{h_t} is $<$ -70 dB and -100 dB due to dynamic traffic during the rush and late hours. Additive attenuation due to weather conditions causes further reductions of μ_{h_t}, and hence, its impact becomes negligible.

V. Conclusions

This paper has calculated the average channel capacity upper bound using the sphere packing and constraint relaxation and lower bound by assuming a channel input with a truncated-exponential or truncated Gaussian distribution. We also considered a channel model that accounted for the impact of dynamic traffic during the rush and late hours, atmospheric turbulence, haze and fog as well as constraints on the peak and average transmitted optical power for safety and practical considerations. The results demonstrated that higher average capacity of 0.7 bit/s/Hz was achievable during rush hours compared to the late hours and with a negligible impact of weather conditions. The constraint relaxation and the truncated-exponential distribution methods provided tight

bounds with a minimum gap of 0.4 bit/s/Hz during the rush hours and under the clear weather condition. Tighter channel bounds can be achieved by finding an optimal channel input distribution. In addition, the study revealed that the V2V-VLC channel variation is influenced by the dynamic traffic environment. Hence to overcome channel variation, adaptive transmission and reception techniques are required.

ACKNOWLEDGEMENTS

The authors would like to thank the National Highways for providing traffic data. The DSP centre of excellence has been part-funded by the European Regional Development Fund through Welsh Government and also by the North Wales Growth Deal through Ambition North Wales, Welsh Government and UK Government. This work is also supported by the EU Cost Action NEWFOCUS CA19111.

REFERENCES

[1] G.-P. Antonio and C. Maria-Dolores, "Multi-agent deep reinforcement learning to manage connected autonomous vehicles at tomorrow's intersections," *IEEE Transactions on Vehicular Technology*, vol. 71, no. 7, pp. 7033–7043, 2022.

[2] X. You, C.-X. Wang, J. Huang, X. Gao, Z. Zhang, M. Wang, Y. Huang, C. Zhang, Y. Jiang, J. Wang *et al.*, "Towards 6G wireless communication networks: vision, enabling technologies, and new paradigm shifts," *Sci. China Inf. Sci.*, vol. 64, no. 1, pp. 1–74, Jan. 2021.

[3] M. Uysal, Z. Ghassemlooy, A. Bekkali, A. Kadri, and H. Menouar, "Visible light communication for vehicular networking: Performance study of a V2V system using a measured headlamp beam pattern model," *IEEE Veh. Technol. Mag.*, vol. 10, no. 4, pp. 45–53, Dec. 2015.

[4] B. Béchadergue, L. Chassagne, and H. Guan, "Simultaneous visible light communication and distance measurement based on the automotive lighting," *IEEE Trans. Intell. Veh.*, vol. 4, no. 4, pp. 532–547, Aug. 2019.

[5] J. Chen and Z. Wang, "Topology control in hybrid VLC/RF vehicular Ad-Hoc network," *IEEE Trans. Wireless Commun.*, vol. 19, no. 3, pp. 1965–1976, Mar. 2020.

[6] S. Rehman, S. Ullah, P. Chong, S. Yongchareon, and D. Komosny, "Visible light communication: a system perspective—overview and challenges," *Sensors*, vol. 19, no. 5, p. 1153, Mar. 2019.

[7] P. Sharda, M. R. Bhatnagar, and Z. Ghassemlooy, "Modeling of a vehicle-to-vehicle based visible light communication system under shadowing and investigation of the diversity-multiplexing tradeoff," *IEEE Transactions on Vehicular Technology*, pp. 1–1, 2022.

[8] F. M. Alsalami, Z. Ahmad, S. Zvanovec, P. A. Haigh, O. C. Haas, and S. Rajbhandari, "Statistical channel modelling of dynamic vehicular visible light communication system," *Veh. Commun.*, vol. 29, p. 100339, June 2021.

[9] M. Karbalayghareh, F. Miramirkhani, H. B. Eldeeb, R. C. Kizilirmak, S. M. Sait, and M. Uysal, "Channel modelling and performance limits of vehicular visible light communication systems," *IEEE Transactions on Vehicular Technology*, pp. 1–1, 2020.

[10] H. Abuella, F. Miramirkhani, S. Ekin, M. Uysal, and S. Ahmed, "ViLDAR—visible light sensing-based speed estimation using vehicle headlamps," *IEEE Trans. Veh. Technol.*, vol. 68, no. 11, pp. 10 406–10 417, 2019.

[11] E. Eso, Z. Ghassemlooy, S. Zvanovec, J. Sathian, M. M. Abadi, and O. I. Younus, "Performance of vehicular visible light communications under the effects of atmospheric turbulence with aperture averaging," *Sensors*, vol. 21, no. 8, 2021. [Online]. Available: https://www.mdpi.com/1424-8220/21/8/2751

[12] Z. Ghassemlooy, W. Popoola, and S. Rajbhandari, *Optical wireless communications: system and channel modelling with Matlab®*. Boca Raton, FL: CRC Press (Inc.), 2019.

[13] M. A. Khalighi and M. Uysal, "Survey on free space optical communication: A communication theory perspective," *IEEE Communications Surveys and Tutorials*, vol. 16, no. 4, pp. 2231–2258, 2014.

[14] K. P. Peppas, A. N. Stassinakis, H. E. Nistazakis, and G. S. Tombras, "Capacity analysis of dual amplify-and-forward relayed free-space optical communication systems over turbulence channels with pointing errors," *J. Opt. Commun. Netw.*, vol. 5, no. 9, pp. 1032–1042, Sep 2013.

[15] H. E. Nistazakis, E. A. Karagianni, A. D. Tsigopoulos, M. E. Fafalios, G. S. Tombras, and S. Member, "Average capacity of optical wireless communication systems over atmospheric turbulence channels," *in Journal of Lightwave Technology*, vol. 27, no. 8, pp. 974–979, 2009.

[16] F. Benkhelifa, Z. Rezki, and M.-S. Alouini, "Low SNR capacity of FSO links over gamma-gamma atmospheric turbulence channels," *IEEE Communications Letters*, vol. 17, no. 6, pp. 1264–1267, 2013.

[17] I. E. Lee, Z. Ghassemlooy, W. P. Ng, and M. Uysal, "Performance analysis of free space optical links over turbulence and misalignment induced fading channels," in *2012 8th International Symposium on Communication Systems, Networks and Digital Signal Processing (CSNDSP)*, 2012, pp. 1–6.

[18] K. Xu, H. Y. Yu, Y. J. Zhu, and Y. Sun, "On the ergodic channel capacity for indoor visible light communication systems," *IEEE Access*, vol. 5, pp. 833–841, 2017.

[19] A. Lapidoth, S. M. Moser, and M. A. Wigger, "On the capacity of free-space optical intensity channels," *IEEE Transactions on Information Theory*, vol. 55, no. 10, pp. 4449–4461, 2009.

[20] S. Hranilovic and F. Kschischang, "Capacity bounds for power- and band-limited optical intensity channels corrupted by Gaussian noise," *IEEE Transactions on Information Theory*, vol. 50, no. 5, pp. 784–795, 2004.

[21] A. A. Farid and S. Hranilovic, "Capacity bounds for wireless optical intensity channels with Gaussian noise," *IEEE Transactions on Information Theory*, vol. 56, no. 12, pp. 6066–6077, 2010.

[22] J. Wang, Q. Hu, J. Wang, M. Chen, and J. Wang, "Tight bounds on channel capacity for dimmable visible light communications," *Journal of Lightwave Technology*, vol. 31, no. 23, pp. 3771–3779, 2013.

[23] R. Jiang, Z. Wang, Q. Wang, and L. Dai, "Upper bound on channel capacity for visible light communications," *IEEE Communications Letters*, vol. 20, no. 1, pp. 97–100, 2016.

[24] A. Chaaban, J.-M. Morvan, and M.-S. Alouini, "Free-space optical communications: Capacity bounds, approximations, and a new sphere-packing perspective," *IEEE Transactions on Communications*, vol. 64, no. 3, pp. 1176–1191, 2016.

[25] T. Chan, S. Hranilovic, and F. Kschischang, "Capacity-achieving probability measure for conditionally Gaussian channels with bounded inputs," *IEEE Transactions on Information Theory*, vol. 51, no. 6, pp. 2073–2088, 2005.

[26] J.-Y. Wang, X.-T. Fu, R.-R. Lu, J.-B. Wang, M. Lin, and J. Cheng, "Tight capacity bounds for indoor visible light communications with signal-dependent noise," *IEEE Transactions on Wireless Communications*, vol. 20, no. 3, pp. 1700–1713, 2021.

[27] J. Vučič, C. Kottke, S. Nerreter, K. Langer, and J. W. Walewski, "513 Mbit/s visible light communications link based on DMT-modulation of a white LED," *Journal of Lightwave Technology*, vol. 28, no. 24, pp. 3512–3518, 2010.

[28] H. Chun, S. Rajbhandari, G. Faulkner, D. Tsonev, E. Xie, J. J. D. McKendry, E. Gu, M. D. Dawson, D. C. O'Brien, and H. Haas, "LED based wavelength division multiplexed 10 Gb/s visible light communications," *Journal of Lightwave Technology*, vol. 34, no. 13, pp. 3047–3052, 2016.

[29] M. A. Arfaoui, M. D. Soltani, I. Tavakkolnia, A. Ghrayeb, M. Safari, C. Assi, and H. Haas, "Physical layer security for visible light communication systems: A survey," *IEEE Communications Surveys Tutorials*, pp. 1–1, 2020.

[30] F. M. Alsalami, N. Aigoro, A. Mahmoud, Z. Ahmad, P. A. Haigh, O. C. Haas, and S. Rajbhandari, "Impact of vehicle headlights radiation pattern on dynamic vehicular visible light communication system channel," *J. Lightw. Technol.*, vol. Early Access, pp. 1–1, 2021.

[31] M. A. Esmail, H. Fathallah, and M. Alouini, "Outage probability analysis of FSO links over foggy channel," *IEEE Photon. J.*, vol. 9, no. 2, pp. 1–12, Apr. 2017.

[32] A. Chaaban, Z. Rezki, and M.-S. Alouini, "On the capacity of intensity-modulation direct-detection Gaussian optical wireless communication channels: A tutorial," *IEEE Communications Surveys and Tutorials*, vol. 24, no. 1, pp. 455–491, 2022.

[33] A. Chen, H. Wu, Y. Wei, and H. Tsai, "Time variation in vehicle-to-vehicle visible light communication channels," in *2016 IEEE Vehicular Networking Conference (VNC)*, Dec 2016, pp. 1–8.

[34] S. Lee, J. K. Kwon, S.-Y. Jung, and Y.-H. Kwon, "Evaluation of visible light communication channel delay profiles for automotive applications," *EURASIP journal on Wireless Communications and Networking*, vol. 2012, no. 1, p. 370, 2012.

[35] A. Memedi, H. Tsai, and F. Dressler, "Impact of realistic light radiation pattern on vehicular visible light communication," in *Proc. 2017 IEEE*

Global Commun. Conf. (GLOBECOM'17), Singapore, Dec. 2017, pp. 1–6.

[36] Hua-Yen Tseng, Y. Wei, Ai-Ling Chen, Hao-Ping Wu, Hsuan Hsu, and H. Tsai, "Characterizing link asymmetry in vehicle-to-vehicle visible light communications," in *Proc. 2015 IEEE VNC*, 2015, pp. 88–95.

[37] I. I. Kim, B. McArthur, and E. Korevaar, "Comparison of laser beam propagation at 785 nm and 1550 nm in fog and haze for optical wireless communications," in *SPIE Optics East*, 2001.

[38] Y. H. Kim, W. A. Cahyadi, and Y. H. Chung, "Experimental demonstration of VLC-based vehicle-to-vehicle communications under fog conditions," *IEEE Photon. J.*, vol. 7, no. 6, pp. 1–9, Dec. 2015.

[39] G.-y. Hu, C.-y. Chen, and Z.-q. Chen, "Free-space optical communication using visible light," *Journal of Zhejiang University - Science A: Applied Physics & Engineering*, vol. 8, pp. 186–191, Feb 2007.

[40] A. Papoulis, S. Pillai, and S. Pillai, *Probability, Random Variables, and Stochastic Processes*. McGraw-Hill (Inc.), New York, NY, USA, 2002.

[41] I. E. Lee, Z. Ghassemlooy, W. P. Ng, and M. Uysal, "Performance analysis of free space optical links over turbulence and misalignment induced fading channels," in *2012 8th International Symposium on Communication Systems, Networks and Digital Signal Processing (CSNDSP)*, 2012, pp. 1–6.

[42] T. M. Cover and J. A. Thomas, *Elements of information theory*, 2nd ed. Hoboken, N.J.: Wiley-Interscience, 2006.

[43] A. Laourine, A. Stephenne, and S. Affes, "On the capacity of log-normal fading channels," *IEEE Transactions on Communications*, vol. 57, no. 6, pp. 1603–1607, 2009.

[44] R. Jiang, Z. Wang, Q. Wang, and L. Dai, "A tight upper bound on channel capacity for visible light communications," *IEEE Communications Letters*, vol. 20, no. 1, pp. 97–100, 2016.

APPENDIX

A. Convergence analysis for infinite series expressions

The first term in (18), (19), (23), and (32) is infinite series expression. To find the convergence, this term is rewritten as follows:

$$\begin{aligned}
&\sum_{k=1}^{+\infty}\frac{(-1)^{k+1}}{k}\left[\operatorname{erfcx}\left(\frac{\sigma k}{\sqrt{2}}+\frac{\mu}{\sqrt{2}\sigma_{h_t}}\right)+\operatorname{erfcx}\left(\frac{\sigma k}{\sqrt{2}}-\frac{\mu}{\sqrt{2}\sigma_{h_t}}\right)\right]\\
&=\underbrace{\sum_{k=1}^{+K}\frac{(-1)^{k+1}}{k}\left[\operatorname{erfcx}\left(\frac{\sigma k}{\sqrt{2}}+\frac{\mu}{\sqrt{2}\sigma_{h_t}}\right)+\operatorname{erfcx}\left(\frac{\sigma k}{\sqrt{2}}-\frac{\mu}{\sqrt{2}\sigma_{h_t}}\right)\right]}_{A}\\
&+\underbrace{\sum_{k=K+1}^{+\infty}\frac{(-1)^{k+1}}{k}\left[\operatorname{erfcx}\left(\frac{\sigma k}{\sqrt{2}}+\frac{\mu}{\sqrt{2}\sigma_{h_t}}\right)+\operatorname{erfcx}\left(\frac{\sigma k}{\sqrt{2}}-\frac{\mu}{\sqrt{2}\sigma_{h_t}}\right)\right]}_{B}
\end{aligned} \tag{33}$$

where μ denotes μ_e, μ_d , μ_j or μ_u in (18), (19), (23), and (32), respectively.

Considering a sufficiently large value of K, in the second term B, $\operatorname{erfcx}(x)$ diverges to $\operatorname{erfcx}(x) \simeq \frac{1}{x\sqrt{\pi}}$. Hence, the second term B is reduced to [43]:

$$B = \frac{2}{\sigma\sqrt{2\pi}}\sum_{k=K+1}^{+\infty}\frac{(-1)^{k+1}}{k(k+\frac{\mu}{\sigma_{h_t}^2})}+\sum_{k=K+1}^{+\infty}\frac{(-1)^{k+1}}{k(k-\frac{\mu}{\sigma_{h_t}^2})} \tag{34}$$

When $\mu > 0$ the term B diverges to [43]:

$$B=\frac{2\sigma_{h_t}}{\mu\sqrt{2\pi}}(-1)^K\left[\beta\Big(K+1-\frac{\mu}{\sigma_{h_t}^2}\Big)-\beta\Big(K+1+\frac{\mu}{\sigma_{h_t}^2}\Big)\right] \tag{35}$$

where $\beta(\cdot)$ is given by [43]:

$$\beta(x)=\frac{1}{2}\left(\frac{d}{dx}\ln\Gamma\Big(\frac{x+1}{2}-\frac{d}{dx}\Big)-\ln\Gamma\Big(\frac{x}{2}\Big)\right) \tag{36}$$

where $\Gamma(\cdot)$ is the Gamma function.